




Development and production of a CNC machined 420 stainless steel reinforced with Cu by hot pressing

A. Cunha^{1,2,*} , J. Pinto^{1,2}, M. F. Cerqueira^{3,4}, F. S. Silva^{1,2}, B. Trindade⁵, and O. Carvalho^{1,2}

¹CMEMS – Center for MicroElectroMechanical Systems, University of Minho, 4800-058 Guimarães, Portugal

²LABBELS – Associate Laboratory, Braga/Guimarães, Portugal

³Centro de Física, University of Minho, 4710-057 Braga, Portugal

⁴International Iberian Nanotechnology Laboratory (INL), Av. Mestre José Veiga S/N, 4715-330 Braga, Portugal

⁵CEMMPRE – Center for Mechanical Engineering, Materials and Processes, University of Coimbra, 3030-788 Coimbra, Portugal

Received: 24 November 2022

Accepted: 19 February 2023

Published online:

8 March 2023

© The Author(s) 2023

ABSTRACT

Multi-material structures make it possible to obtain effective solutions to engineering problems by combining the benefits of different materials to meet the requirements of different working conditions. The aim of this multifunctional 420 stainless steel-copper structure is to create a hybrid solution in which copper acts as heat-transfer enhancer (through cooling channels) while maintaining the required mechanical properties of the steel matrix. This work focuses on a combined engineering process consisting of CNC machining through holes on a 420 stainless steel surface substrate and subsequent filling with copper by hot pressing. The influence of the copper filling on the physical, chemical, microstructural, mechanical, and thermal properties of this multi-material solution was analysed. The machined area (5% of the total surface area) consisted of nine holes with a diameter of approximately 1 mm. The multi-material samples showed high densification, homogeneous microstructures, and a well-defined and sharp interface between the two materials. The microhardness values measured for the 420 stainless steel and copper were 759 and 57 HV, respectively, and the thermal conductivity of the multi-material was $\cong 59\%$ higher than the 420 stainless steel (39.74 and 16.40 W/m K, respectively).

Introduction

The rapid development of engineering applications associated with extreme working conditions makes it increasingly difficult to use single-material parts fabricated by traditional methods [1]. Furthermore,

currently, components are required to have multi-functional and multi-environmental adaptation characteristics [1, 2]. Multi-material solutions make it possible to obtain remarkable final properties by combining the benefits of different materials to meet the requirements of different working conditions

Handling Editor: Sophie Primig.

Address correspondence to E-mail: a.cunha@dem.uminho.pt

[1, 3–5]. Multi-material structures have an important potential for application in different fields namely: aerospace, automotive, electronic component, nuclear, and other industries [1, 2, 6]. Particularly, steel-copper multi-material structures have recently been studied due to their ability to offer unique solutions to engineering problems when compared to traditionally fabricated single-material structures [1, 2, 4]. Different studies about steel-copper multi-material solutions produced by different techniques have been reported in the literature. Cunha et al. [3] developed a multi-material consisting of 420 stainless steel-copper parts fabricated by 3D multi-material laser powder bed fusion to improve the heat extraction of a plastic injection mould. Tan et al. [7] produced a maraging steel-copper functional bimetal combining additive and subtractive processes to study the interfacial metallurgical bonding mechanism and the evolution of interfacial microstructures. However, there are some difficulties in combining steel and copper alloys, due to their different physical and chemical properties. In addition to the quite low solubility between Fe and Cu and the absence of intermetallic phases in the Fe–Cu phase diagram, there is a significant difference in the values of the thermal expansion coefficient and thermal conductivity between these materials, which leads to a large deformation and residual stresses in the joint [3, 7–9]. In fact, 420 stainless steel is a martensitic steel with a high chromium content (more than 11 wt.%), providing high mechanical and corrosion properties suitable for surgical tools, razor blades, bearings, the marine and aerospace industries, and plastic injection moulds [10–14]. However, it presents some limitations when good tribological properties are required or in applications where thermal conductivity/heat extraction is an important issue as in plastic injection moulds, for example [3, 15]. To solve the problem associated with its low thermal conductivity ($\cong 25 \text{ W/m K}$), copper and its alloys are suitable candidates. However, it is important to mention that although pure copper presents a high thermal conductivity ($\cong 400 \text{ W/m K}$), it is a very ductile material, and for this reason, its use in the production of the mould's core and cavity might limit its working lifetime [16, 17].

The present work focuses on the development of a combined engineering process for the development of a novel 420 stainless steel-copper multifunctional surface consisting of CNC machining through holes on a steel surface substrate and subsequent filling

with copper by hot pressing (HP). The aim is to create a hybrid multi-material solution in which copper, due to its excellent thermal conductivity, reinforces heat-transfer while the steel alloy matrix ensures the mechanical properties necessary. It is expected that the simultaneous application of temperature and pressure might lead to an improved metallurgical and mechanical bond between the two materials when compared to previous work on this system [3]. In a previous study on the manufacturing of 420 stainless steel-copper components made by laser surface patterning of steel and subsequent filling with copper by hot pressing [18], the authors have shown that the thermal properties of the 420 stainless steel were improved, with a high potential to be used in plastic injection moulds. The novelty of the solution that is now proposed concerns the creation of heat flow channels by machining holes in the steel and the consequent consolidation of copper in these holes by hot pressing. This is a simpler process that does not require texturing the steel. However, due to the depth of the holes, it was necessary to increase the sintering temperature (to $1080 \text{ }^\circ\text{C}$), to ensure that the copper was in a liquid enough state to fill the holes entirely. This may lead to a better bond between the steel and copper as well as reduce the number of pores at the copper grain boundary.

Materials and methods

CNC machining

Samples of 420 stainless steel (420SS), annealed at $880 \text{ }^\circ\text{C}$, with a diameter of 14 mm and a thickness of 4 mm were CNC machined using Kern Micromachine equipment, the NC HEIDENHAIN TNC 415 controller. This machine has a high-frequency spindle that varies between 315 and 20,000 rpm, maximum power of 1.80 kW, and maximum torque of 0.9 N m. Moreover, it includes an electronic crank handle swerved, a continuous variation in frequency converter for the high-frequency spindle, and a lubricating tank with a pump.

The process starts with the machining of an aluminium support (AW-2007 aluminium alloy) in which the 420 stainless steel samples will be fixed (Fig. 1). The rip was milled with a 5 mm one-edge flat tip end mill (Fig. 1a). Subsequently, the hole for fixing the 420 stainless steel samples, with a depth of

3.9 mm, was machined using the same end mill and machining parameters (Fig. 1b). Finally, two small holes were made (Fig. 1c) to ensure the correct fixation (without vibration) of the samples with screws during the machining process.

The 420 stainless steel samples were fixed to the support shown in Fig. 1 and nine 1 mm through holes were machined (Fig. 2). The holes were made with a 0.8 mm ball nose end mill while applying a feed rate of 2 mm/min and spindle speed of 20,000 rpm. This operation was carried out up to a penetration of 5 mm to guarantee perfect machining of the holes.

Hot pressing

After the CNC machining, copper powder (TLS Technik, average particle size 15–45 μm and 99.9% purity) was consolidated and sintered in the 420SS machined holes by hot pressing. The hot pressing was conducted using a pressure-assisted sintering system (under a vacuum of 10^{-2} mbar) with a high-frequency induction furnace (Fig. 3). The samples were heated up to 1080 $^{\circ}\text{C}$ (melting point of the copper), with a heating rate of 100 $^{\circ}\text{C}/\text{min}$, a pressure of 65 MPa was applied for 30 min, followed by cooling down to room temperature. It is important to mention that to compensate for the contraction of the copper powder during the sintering process, not only were the holes of the CNC machining sample completely covered with the powder before hot pressing but the surface was also completely covered with copper to compensate for the shrinkage of the powder during the HP process. The graphite die was placed inside the chamber, where both temperature and pressure were increased till reaching the targeted

values and these conditions were maintained during this stage.

After hot pressing processing, the 420SS-copper samples were polished with silicon carbide abrasive papers down to a 4000 mesh and ultrasonically cleaned in an isopropyl alcohol (IPA) bath for 10 min before their characterisation. This exposed the machined steel surface. The commercial 420 stainless steel sample was also included in this study as a reference.

Characterisation techniques

The samples were analysed by scanning electron microscopy (SEM) (Nano-SEM-FEI Nova 200 equipment) with electron dispersive spectroscopy (EDS) (EDAX-Pegasus X4M). X-ray diffraction (XRD) phase analysis was conducted using a PANalytical X'Pert PRO MPD equipment with Co $K\alpha$ radiation. Vickers hardness was evaluated with a microhardness tester (DuraScan of EMCO-TEST). Twenty indentations were made along the top surface of the multi-material (ten in each material) under an applied load of 100 gf and a dwell time of 20 s. Nanohardness tests were also performed close to the 420SS-copper interface (area of $80 \times 80 \mu\text{m}^2$, corresponding to 100 measurements) by depth-sensing indentation (MicroMaterials NanoTest) with an applied load of 3 mN.

The four-point technique (Fig. 4) was used to assess the electrical resistivity (ρ) of the mono- (commercial 420SS) and multi-material samples, with the probes located on the 420SS surface (five measurements). This technique consists on the application of a current (I) through the specimen and simultaneously measuring the resultant voltage (V) produced. The electrical resistivity of the material is then obtained using the following equation:

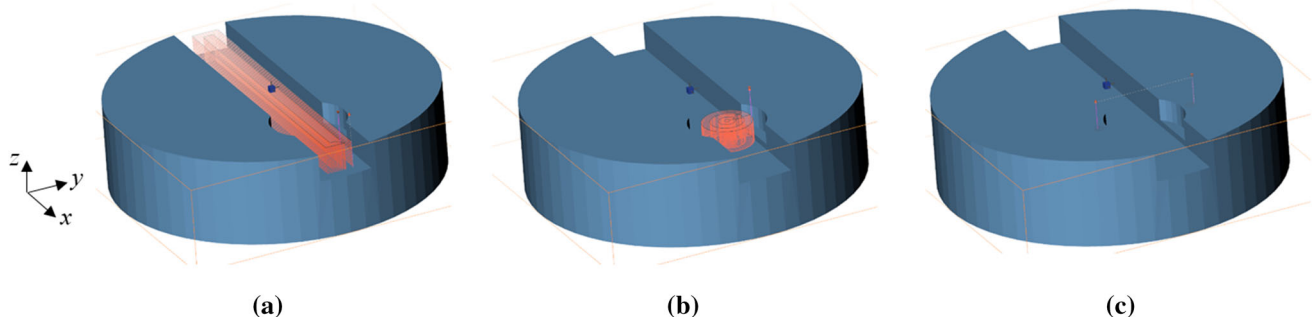


Figure 1 Aluminium support: **a** rip, **b** hole for fixing the 420 stainless steel samples, and **c** small holes to screw the 420 stainless steel samples in position.

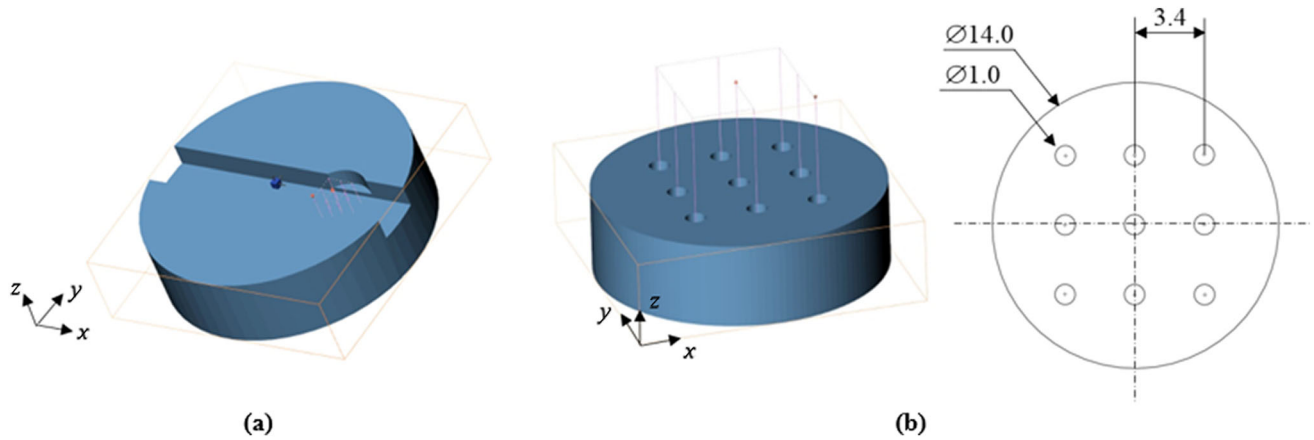


Figure 2 420 stainless steel samples machining: **a** aluminium support, and **b** machining design and strategy.

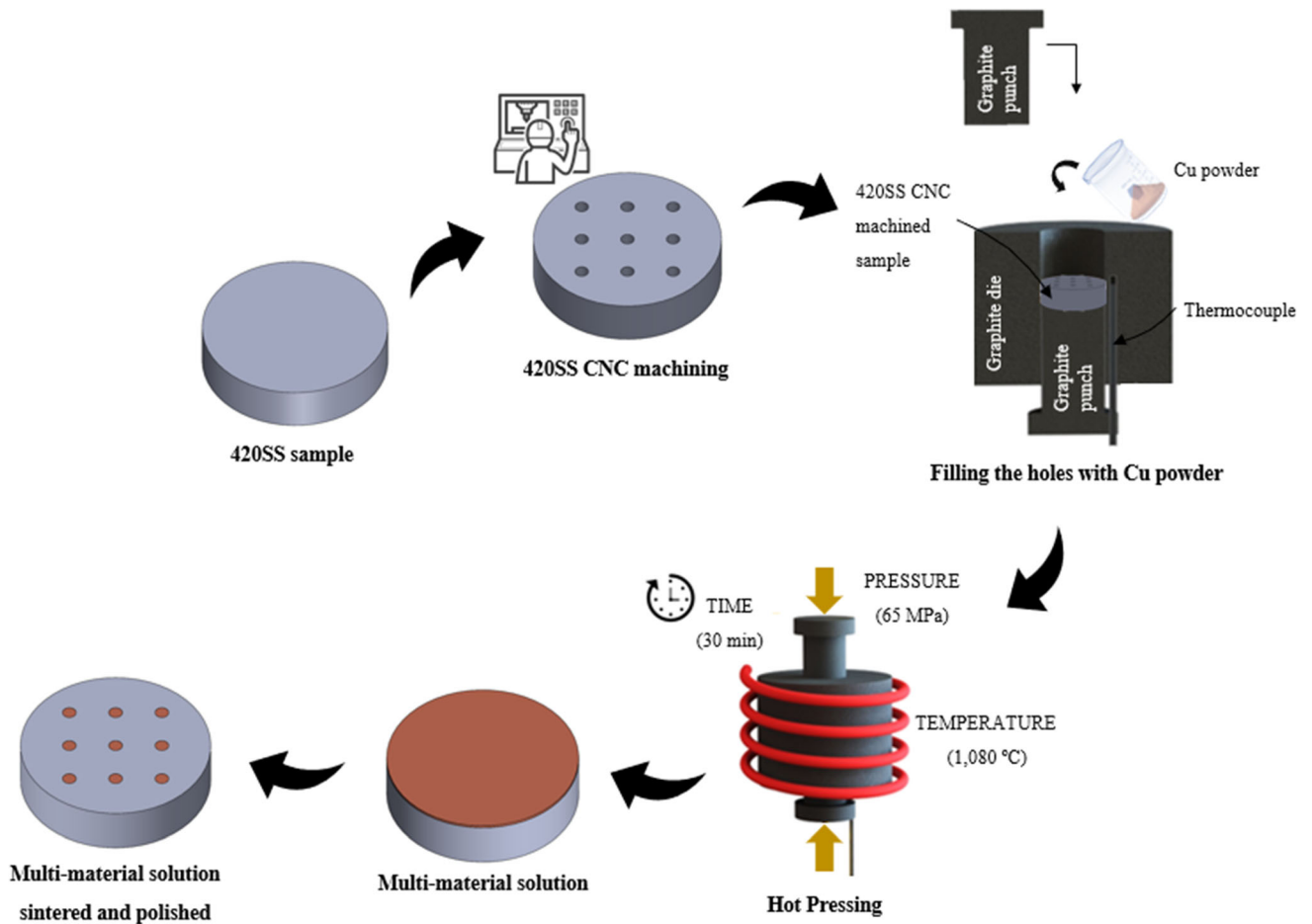


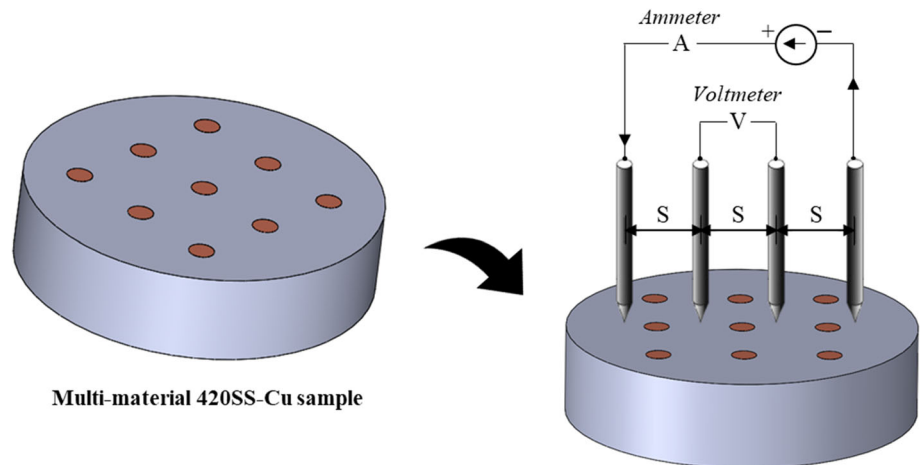
Figure 3 Schematic representation of the process used for the production of the 420 stainless steel-copper solution.

$$\rho = 2\pi \times S \times \frac{V}{I} \tag{1}$$

where ρ is the electrical resistivity in Ω m, S is the distance between the two inner contacts/probes in m, V is the voltage in V, and I is the current in A.

The electrical resistivity was correlated to the thermal conductivity (k) through the Wiedemann–Franz law (Eq. 2) [19, 20]. This law is valid for materials with relatively high thermal conductivity,

Fig. 4 Schematic representation of the four-point technique apparatus used to measure the electrical resistivity of the samples produced.



in which the electron contribution is higher than the phonon contribution.

$$k = \frac{L \times T}{\rho} \quad (2)$$

where k is the thermal conductivity in W/m K, L is the Lorenz number ($2.44 \times 10^{-8} \text{ W } \Omega/\text{K}^2$), and T is the temperature in K. The temperature considered was room temperature (298 K).

The rule of mixture (Eq. 3) was used to estimate the theoretical thermal conductivity ($k_{420SS-Cu}$) value of the multi-material samples and compare it with the experimental value obtained.

$$k_{420SS-Cu} = V_{420SS} \times k_{420SS} + V_{Cu} \times k_{Cu} \quad (3)$$

where V is the volume in m^3 . Moreover, the thermal conductivity experimental value of the 420 stainless steel was compared with the value in the literature [21].

Results and discussion

CNC machining

Figure 5a and b shows SEM images of the machined 420 stainless steel. Nine through holes with a mean diameter of approximately $959.4 \pm 38.6 \mu\text{m}$ were drilled corresponding to a machined area of approximately 5%. It is possible to state the uniformity of the holes, as well as their good definition by examining Fig. 5. Furthermore, no changes were observed in the morphology of the areas adjacent to the holes.

Hot pressing

The morphology of the multi-material produced is shown in Fig. 6. It is possible to observe that the diameter of the machined holes decreases by about 10% after the hot pressing process (final diameter of $865.7 \pm 27.3 \mu\text{m}$), due to thermal contraction during the cooling process. The high pressure used led to the plastic deformation of the 420 stainless steel and consequently forced the copper to fill the machined holes. This process was similar to die-casting, in which the high pressure exerted forces the liquid phase to fill a cavity. Moreover, the 420 stainless steel-copper multi-material display high densification, homogeneous microstructures, and a well-defined interface, with no visible diffusion zone. Although an additional volume of copper was added to compensate for the shrinkage of the powder during the process, some porosity is evident in the connection zone between the two materials. It is possible to differentiate the areas of the 420 stainless steel from those of the copper in Fig. 6 since the interfaces between both materials are well defined. At $1080 \text{ }^\circ\text{C}$, the processing temperature of the multi-material samples, copper is in the liquid phase, while the 420 stainless steel is in the solid phase (melting point of $\cong 1500 \text{ }^\circ\text{C}$). Therefore, sintering occurs in the liquid phase enhancing the diffusion of the main elements of the 420 stainless steel (C, Fe and Cr) to the liquid copper phase and vice versa, leading to a suitable metallurgical bonding between the two materials.

From Fig. 6, it is also possible to observe some microcracks and porosities along the interface of the two materials, which can be justified by the significant difference between the values of thermal expansion

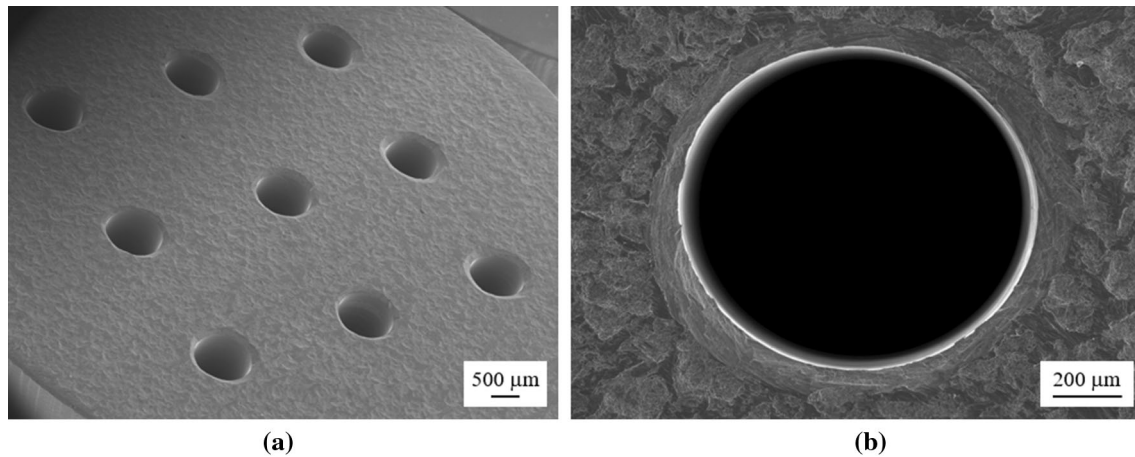


Figure 5 Secondary electron SEM images of the machined 420 stainless steel: **a** distribution of the holes drilled in the sample, and **b** detail of the machined hole.

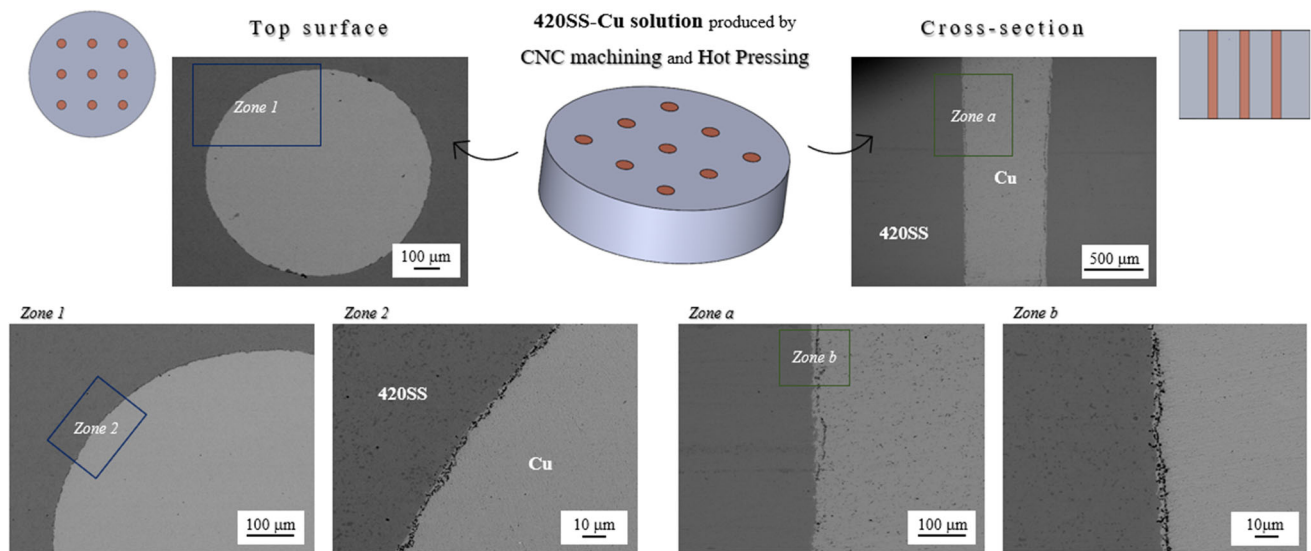


Figure 6 Surface morphology of the multi-material 420SS-Cu solution produced by CNC machining and Hot Pressing (top surface and cross section).

coefficients presented by the two materials, the 420 stainless steel ($\cong 9\text{--}11 \mu\text{m}/\text{m K}$ from 0 to 1000 °C) [22] and copper ($\cong 17\text{--}20 \mu\text{m}/\text{m K}$ from 0 to 1000 °C) [23]. Furthermore, pure copper has been reported as a material that is hard to cast, since it is susceptible to surface cracking, shrinkage, and internal defects [24]. Generally, multi-material samples display thermal stresses when subjected to temperature variations, due to the difference in the thermal expansion coefficients of the materials that constitute them. This difference can induce the occurrence of several defects in the interface, namely the formation of microcracks and/or pores, leading to a thermally imperfect interface with

lower heat conductivity [25]. It is important to note that the interface cracks may be thermally insulative and the bonding interface tends to be thermally perfect and therefore, no heat flows across the crack [25]. Another possibility for the emergence of cracks at the interface could be related to the diffusion of copper resulting in the embrittlement of the austenitic grain boundaries [3, 26]. Although some defects have been reported in studies related to this pair of materials, Joshi et al. [27] showed that it is possible to obtain stainless steel-copper bimetallic joints by hot pressing without evidence of cracking on the interface after thermal cycling.

EDS analysis was performed along a line, which included regions of steel and copper on the sample surface (Fig. 7). The EDS mapping shows a narrow interface region of $\sim 2 \mu\text{m}$ wide (position 70.5–72.5 μm) between the steel alloy and copper. This means that no significant atomic diffusion occurred between the two materials, meaning that the individual final properties of each material are guaranteed.

The XRD patterns of the annealed 420SS (raw material) and 420SS-copper samples are shown in Fig. 8. In the same image, an optical image of the copper microstructure, with an average grain size of $15 \mu\text{m}$, can be seen. The raw 420 stainless steel is formed by ferrite and chromium carbides, characteristic of the annealed state. The XRD pattern of the hot-pressed 420SS-copper sample shows two phases, one corresponding to Cu and the other to martensite. No carbides were detected after hot pressing. This means that during the hot pressing the maximum temperature reached allowed austenite to form and the dissolution of the chromium carbides present. During the phase of cooling down to room temperature the cooling rate was fast enough to permit the formation of martensite from the austenite phase.

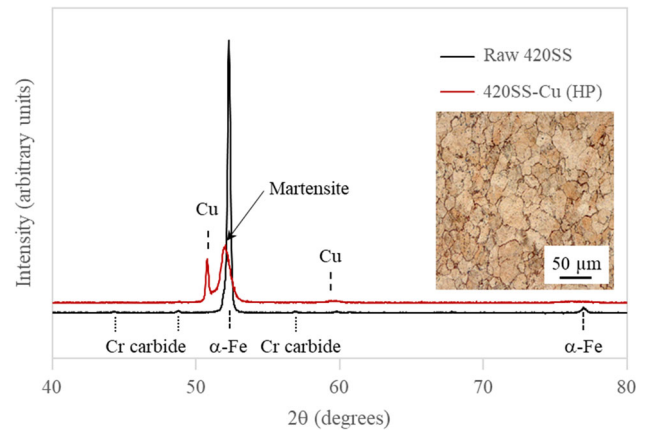


Figure 8 XRD pattern of the annealed 420SS (before hot pressing) and 420SS-copper (after hot pressing) samples, and an optical image of the copper microstructure.

Hardness

Vickers microhardness of the multi-material samples was measured in different regions of the 420 stainless steel and copper, all over the top surface (Fig. 9). The 420 stainless steel hardness was evaluated before (annealed condition) and after hot pressing.

The hardness results of the annealed 420 stainless steel ($228 \text{HV}_{0.1}$) were coherent with those reported in the literature (247HV) [28, 29]. After the hot pressing,

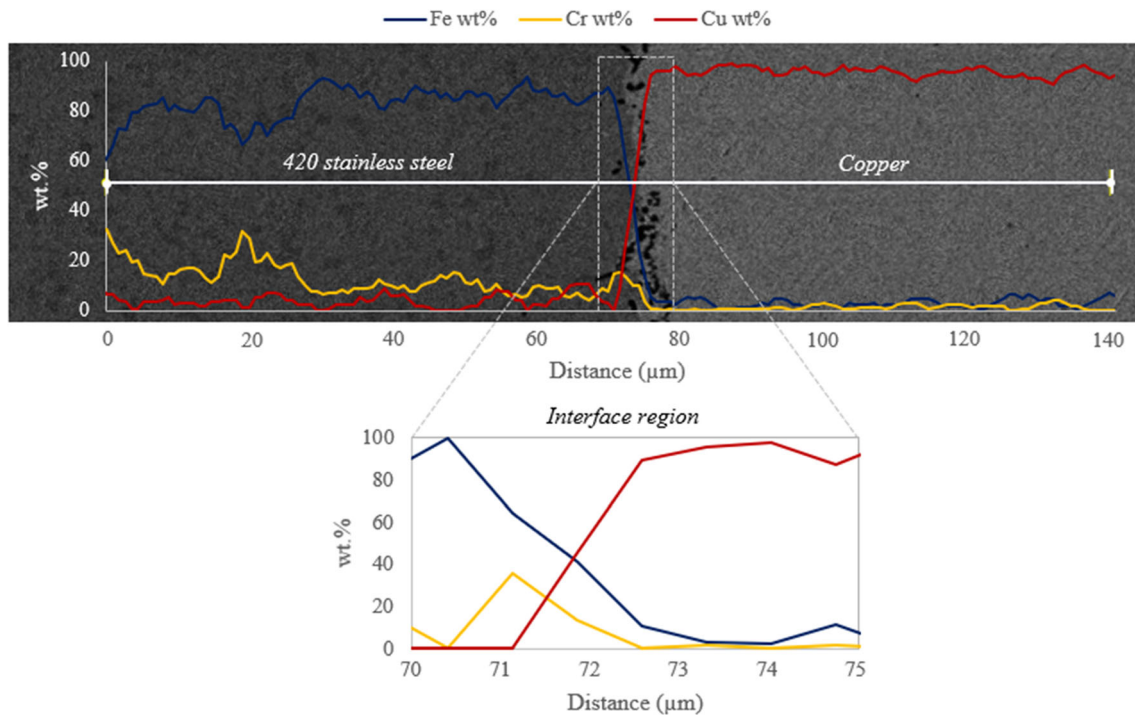


Figure 7 EDS mapping of the multi-material 420 stainless steel-copper sample (top surface).

the hardness of the 420 stainless steel substantially increases (759 HV_{0.1}) due to the dissolution of the carbides at the high temperature, incorporation of carbon into the austenite phase and formation of martensite during cooling. This value is higher than the ones reported for the same steel processed by hot pressing at 960 °C (550 HV) [30] and metal injection moulding (490 HV) [31]. However, the value obtained in this study is similar to those reported for laser powder bed fusion (750 HV) [32, 33] on the inner layers of the parts.

The maximum temperature of the fabrication process affects the final microstructure and the corresponding mechanical properties. The temperature selected for the hot pressing (1080 °C) was 120 °C higher than the one of the Nachum and Fleck [30] study (960 °C). Between these two temperatures, more carbon is incorporated in the austenite phase and consequently, the harder the martensite is after cooling to room temperature.

Concerning the copper region, the hardness values obtained were similar to the ones reported in the literature for the annealed condition (57 HV) [34], and LPBF parts (65 HV) [35], but lower than the one reported by Vikas et al. [36] for pure copper (89–96 HV) hot-pressed at 900 °C (180 °C lower than the temperature applied in this work). In fact, the samples processed by Vikas et al. [36] have a substantially smaller grain size than that observed in this work (Fig. 8). Moreover, the values now obtained for the copper are lower than the ones obtained for the same material sintered by hot pressing at 890 °C [18].

Nanohardness tests were carried out with a load of 3 mN, and the hardness and reduced modulus were calculated (Fig. 10) to assess the mechanical quality of the steel-copper interface and to determine any structural changes occurring in these areas.

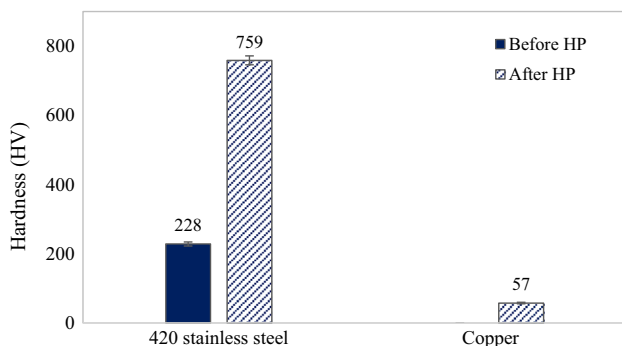


Figure 9 Hardness of the 420 stainless steel and copper before and after hot pressing (HP).

No significant differences in the values of hardness or reduced modulus were obtained close to the interface, meaning that no new structural phases were formed in this region during HP. The mean nanohardness (H) and reduced modulus (E_r) values obtained for the 420SS and copper were 9.09 ± 0.89 GPa, 210 ± 11 GPa (420SS), and 1.22 ± 0.12 GPa, 138 ± 10 GPa (copper), respectively. The highest values obtained for nanohardness when compared to those obtained for microhardness may be explained by the indentation load/size effect (ISE) [37], i.e. they tend to increase with a decreasing indentation load. The same result was obtained by Nachum and Fleck [30] that observed a pronounced size effect on hardness when the contact depth is reduced to the sub-micron level. These authors reported a hardness increase of about 100% for nanoindentation tests when compared to the ones obtained by microindentation (11 and 5.5 GPa, respectively).

Thermal behaviour

The electrical resistivity of the 420 stainless steel and the 420 stainless steel-copper samples was measured using the four-point technique and the thermal conductivity was calculated using the Wiedemann–Franz law (Eq. 2), assuming that heat is transported mainly by conduction electrons [19]. However, electron heat-transfer mechanisms are more efficient than the contribution of phonons since electrons are not as scattered as phonons at higher speeds. Furthermore, the Wiedemann–Franz law considers that the heat transported by the phonons is negligible and the electrons do not suffer inelastic scattering, so there are significant differences between the theoretical value and the real value measured [38]. Thus, the values obtained must be used as a comparison between them to assess the variations induced by the addition of copper and not as a comparison with the theoretical or expected values, since the same conditions were maintained throughout all the tests performed.

Figure 11 shows the experimental electrical and the calculated thermal conductivity of the samples produced. The electrical resistivity obtained for the 420 stainless steel ($44.5 \pm 2.9 \mu\Omega \text{ cm}$) is in accordance with the values reported in the literature ($49\text{--}55 \mu\Omega \text{ cm}$) [39, 40]. The addition of approximately 5% of copper resulted in a significant decrease ($\cong 59\%$) in the electrical resistivity ($18.3 \pm 1.7 \mu\Omega \text{ cm}$) of the multi-material when compared to the 420 stainless

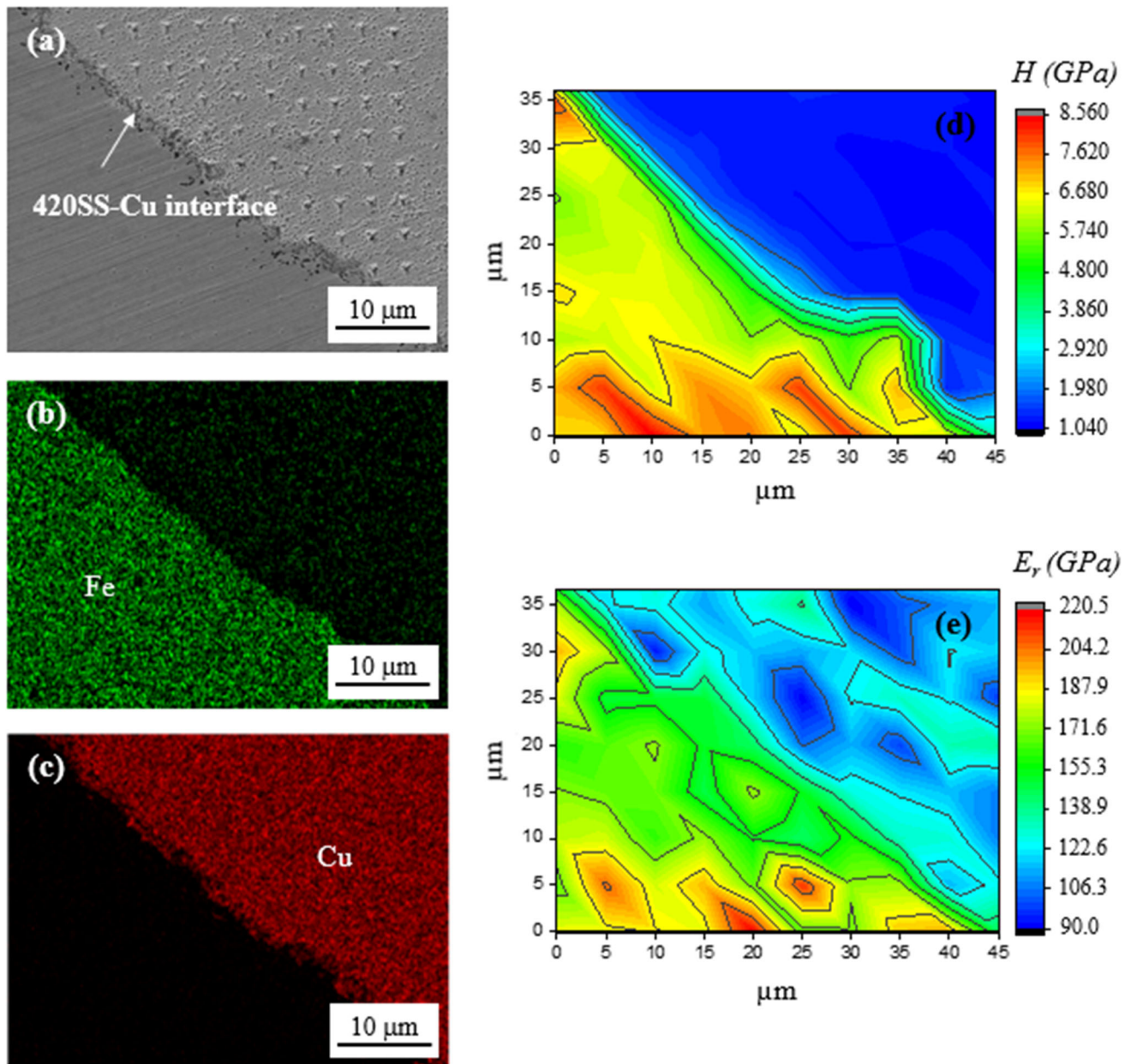


Figure 10 **a** SEM image of the area where the nanoindentation tests were performed, **b** and **c** EDS maps of the same area for Fe and Cu, respectively, **d** nanohardness values map, and **e** reduced modulus map.

steel. Consequently, the thermal conductivity of the 420 stainless steel-copper (39.7 W/m K) HPed sample is considerably higher ($\cong 59\%$) than the only steel (16.4 W/m K), proving the effectiveness in increasing the thermal conductivity of the HPed sample by adding a small amount of copper.

Considering the rule of mixtures (Eq. 3), the thermal conductivity of the multi-material 420 stainless steel-copper samples is about 43.8 W/m K, assuming theoretical values of the thermal conductivity for the

420 stainless steel and copper of 25 and 400 W/m K, respectively [21, 41]. However, it is known that the mixture rule is an overly simplistic model of the bond between two materials since it does not consider interface features or defects that can act as an obstacle to heat conduction [42]. Therefore, the value obtained experimentally (39.7 W/m K) is lower than the theoretical value (43.8 W/m K), possibly due to aspects related to the method of measurement (sample polishing, state of probes, the contact between the

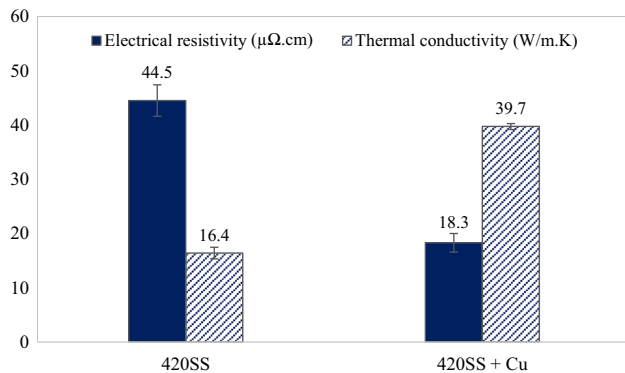


Figure 11 Electrical resistivity and thermal conductivity obtained for the 420 stainless steel and the 420 stainless steel-copper samples.

sample and probe, accuracy, and reproducibility of the system), defects on the interface between the two materials, and also due to the fact that the rule of mixtures is an overly simplistic model of the bond between two materials [43]. In fact, electrons and phonons tend to scatter when trying to cross an interface, as the electronic and vibrational differences between two materials influence the energy carrier [44]. Furthermore, when phonons are being transmitted there is a resistive effect at the interface (interface's resistance to thermal flow) which causes them to be reflected or transmitted. This means that some energy spreads out and so the increase in thermal conductivity is not as significant [45, 46]. Moreover, it is known that the level of densification, as well as defects at the interface (cracks and/or pores) play a major role in the final properties of the samples produced, particularly in the thermal properties [47]. Therefore, Hasselman and Johnson [48] and Nan et al. [49] state that the thermal conductivity of the interface can decrease in the presence of thermal resistance at the bonding interface due to existing pores and microcracks [25]. On the other hand, the authors also claim that the gas trapped in the cracks can make it thermally conductive, so it is important to study the phenomenon of heat-transfer at the interface zone between the two materials.

Conclusions

This study showed that it is possible to improve the thermal properties of 420 stainless steel by a new hybrid multifunctional surface consisting of CNC machined holes on the 420 stainless steel substrate

that were subsequently filled with copper by means of hot pressing. The machined area consisted of nine through holes with a diameter of approximately 1 mm with a machined area of approximately 5%, and the main achievements of the performed study are the following:

- High densification, homogeneous microstructures, and a well-defined interface between steel and copper were achieved by hot pressing.
- XRD analysis concluded that the cooling down after HP was fast enough to transform austenite into martensite.
- Vickers microhardness of the multi-material samples revealed values of 759 HV and 57 HV for the 420 stainless steel and the copper, respectively. The microhardness of the HPed 420 stainless steel was much higher than that of the raw annealed steel due to the formation of martensite. The nanohardness and reduced modulus values obtained for the 420 stainless steel and copper after HP were 9.09 GPa and 210 GPa (420SS) and 1.22 GPa and 138 GPa (copper), respectively. By nanoindentation it was possible to conclude that no significant differences in the values of hardness or reduced modulus were observed close to the 420SS-Cu interface, meaning that no new structural phases were formed during HP.
- Due to the higher thermal conductivity of copper compared to 420SS, its incorporation into the steel was responsible for a 59% of increase in this property (16.4 and 39.7 W/m K for the 420 stainless steel, and the 420 stainless steel-copper multi-material, respectively).

Acknowledgements

This work is supported by FCT (Fundação para a Ciência e a Tecnologia) through the grant SFRH/BD/147460/2019 and the reference projects UIDB/04436/2020 and UIDP/04436/2020, UIDB/00285/2020, and LA/P/0112/2020. Additionally, this work is co-financed by FEDER, through the Competitiveness and Internationalization Operational Program (POCI), in the projects Add. Additive and MoedINOV, with the references POCI-01-0247-FEDER-024533 and POCI-01-0247-FEDER-033361, respectively.



Funding

Open access funding provided by FCT | FCCN (b-on).

Data availability

All data used in this work have been properly cited within the article.

Code availability

Not applicable.

Declarations

Conflict of interest The authors declare that they have no known competing financial interests or personal relationships that could have appeared to influence the work reported in this paper.

Open Access This article is licensed under a Creative Commons Attribution 4.0 International License, which permits use, sharing, adaptation, distribution and reproduction in any medium or format, as long as you give appropriate credit to the original author(s) and the source, provide a link to the Creative Commons licence, and indicate if changes were made. The images or other third party material in this article are included in the article's Creative Commons licence, unless indicated otherwise in a credit line to the material. If material is not included in the article's Creative Commons licence and your intended use is not permitted by statutory regulation or exceeds the permitted use, you will need to obtain permission directly from the copyright holder. To view a copy of this licence, visit <http://creativecommons.org/licenses/by/4.0/>.

References

- [1] Wu X, Zhang D, Yi D et al (2022) Interfacial characterization and reaction mechanism of Ti/Al multi-material structure during laser powder bed fusion process. *Mater Charact* 192:112195. <https://doi.org/10.1016/j.matchar.2022.112195>
- [2] Zhang X, Sun C, Pan T et al (2020) Additive manufacturing of copper–H13 tool steel bi-metallic structures via Ni-based multi-interlayer. *Addit Manuf* 36:101474. <https://doi.org/10.1016/j.addma.2020.101474>
- [3] Cunha A, Marques A, Silva FS et al (2022) 420 stainless steel-Cu parts fabricated using 3D multi-material laser powder bed fusion: a new solution for plastic injection moulds. *Mater Today Commun* 32:103852. <https://doi.org/10.1016/j.mtcomm.2022.103852>
- [4] Onuiké B, Heer B, Bandyopadhyay A (2018) Additive manufacturing of Inconel 718—Copper alloy bimetallic structure using laser engineered net shaping (LENS™). *Addit Manuf* 21:133–140. <https://doi.org/10.1016/j.addma.2018.02.007>
- [5] Zhang X, Pan T, Flood A et al (2021) Investigation of copper/stainless steel multi-metallic materials fabricated by laser metal deposition. *Mater Sci Eng A* 811:141071. <https://doi.org/10.1016/j.msea.2021.141071>
- [6] Zhang X, Li L, Liou F (2021) Additive manufacturing of stainless steel–copper functionally graded materials via Inconel 718 interlayer. *J Mater Res Technol* 15:2045–2058. <https://doi.org/10.1016/j.jmrt.2021.09.027>
- [7] Tan C, Zhou K, Ma W, Min L (2018) Interfacial characteristic and mechanical performance of maraging steel-copper functional bimetal produced by selective laser melting based hybrid manufacture. *Mater Des* 155:77–85. <https://doi.org/10.1016/j.matdes.2018.05.064>
- [8] Guo S, Zhou Q, Kong J et al (2016) Effect of beam offset on the characteristics of copper/304 stainless steel electron beam welding. *Vacuum* 128:205–212. <https://doi.org/10.1016/j.vacuum.2016.03.034>
- [9] Mai TA, Spowage AC (2004) Characterisation of dissimilar joints in laser welding of steel-kovar, copper-steel and copper-aluminium. *Mater Sci Eng A* 374:224–233. <https://doi.org/10.1016/j.msea.2004.02.025>
- [10] Saeidi K, Zapata DL, Lofaj F et al (2019) Ultra-high strength martensitic 420 stainless steel with high ductility. *Addit Manuf* 29:100803. <https://doi.org/10.1016/j.addma.2019.100803>
- [11] Momenzadeh N, Nath SD, Berfield TA, Atre SV (2019) In Situ measurement of thermal strain development in 420 stainless steel additive manufactured metals. *Exp Mech* 59:819–827. <https://doi.org/10.1007/s11340-019-00513-3>
- [12] Cunha A, Marques A, Gasik M, Trindade B (2022) Influence of temperature processing on the microstructure and hardness of the 420 stainless steel produced by hot pressing.

- Mater Manuf Process 38(3):333–340. <https://doi.org/10.1080/10426914.2022.2072885>
- [13] Nath SD, Clinning E, Gupta G et al (2019) Effects of Nb and Mo on the microstructure and properties of 420 stainless steel processed by laser-powder bed fusion. *Addit Manuf* 28:682–691. <https://doi.org/10.1016/j.addma.2019.06.016>
- [14] Nath SD, Okello A, Kelkar R et al (2021) Adapting L-PBF process for fine powders: a case study in 420 stainless steel. *Mater Manuf Process* 37(11):1320–1331. <https://doi.org/10.1080/10426914.2021.1885707>
- [15] Mennig G, Stoeckert K (2013) *Mold-making handbook*, 3rd edn. Hanser Publishers, Munich, pp 679–690
- [16] Reddy KP, Panitapu B (2017) High thermal conductivity mould insert materials for cooling time reduction in thermoplastic injection moulds. *Mater Today Proc* 4:519–526. <https://doi.org/10.1016/j.matpr.2017.01.052>
- [17] Cunha Â, Marques A, Silva MR et al (2022) Laser powder bed fusion of the steels used in the plastic injection mould industry: a review of the influence of processing parameters on the final properties. *Int J Adv Manuf Technol* 121:4255–4287. <https://doi.org/10.1007/s00170-022-09588-0>
- [18] Cunha Â, Marques A, Guimarães B et al (2022) Production of a multi-functional 420 stainless steel-copper surface by laser texturing and hot pressing: a new solution for plastic injection moulds. *Int J Adv Manuf Technol* 123:1341–1352. <https://doi.org/10.1007/s00170-022-10252-w>
- [19] Callister WD, Rethwisch DG (2009) *Materials science and engineering: an introduction*. Wiley, pp 782–799
- [20] Guimarães B, Fernandes CM, Figueiredo D et al (2020) A novel approach to reduce in-service temperature in WC-Co cutting tools. *Ceram Int* 46:3002–3008. <https://doi.org/10.1016/j.ceramint.2019.09.299>
- [21] Korkmaz ME, Günay M (2018) Finite Element modelling of cutting forces and power consumption in turning of AISI 420 martensitic stainless steel. *Arab J Sci Eng* 43:4863–4870. <https://doi.org/10.1007/s13369-018-3204-4>
- [22] States SSI of the U America SSI of N, (Canada) NDI, Institute AI and S (1993) Design guidelines for the selection and use of stainless steel. *Specialty Steel Industry*, pp 32–50
- [23] Wang K, Reeber RR (1943) Thermal expansion of copper alloys. *J Franklin Inst* 236:305–306. [https://doi.org/10.1016/s0016-0032\(43\)90743-4](https://doi.org/10.1016/s0016-0032(43)90743-4)
- [24] Collini L (2012) Copper alloys-early applications and current performance-enhancing processes. *IntechOpen*, pp 1–31
- [25] Wang J, Dai M, Gao CF (2020) The effect of interfacial thermal resistance on interface crack subjected to remote heat flux. *Zeitschrift Angew Math Phys* 71:1–21. <https://doi.org/10.1007/s00033-019-1235-7>
- [26] Magnabosco I, Ferro P, Bonollo F, Arnberg L (2006) An investigation of fusion zone microstructures in electron beam welding of copper-stainless steel. *Mater Sci Eng A* 424:163–173. <https://doi.org/10.1016/j.msea.2006.03.096>
- [27] Joshi GR, Badheka VJ, Darji RS et al (2022) The joining of copper to stainless steel by solid-state welding processes: a review. *Materials (Basel)* 15(20):7234. <https://doi.org/10.3390/ma15207234>
- [28] Sealy MP, Hadidi H, Sotelo LD et al (2020) Compressive behavior of 420 stainless steel after asynchronous laser processing. *CIRP Ann* 69:169–172. <https://doi.org/10.1016/j.cirp.2020.04.059>
- [29] Haghdati N, Laleh M, Moyle M, Primig S (2021) Additive manufacturing of steels: a review of achievements and challenges. *J Mater Sci* 56:64–107. <https://doi.org/10.1007/s10853-020-05109-0>
- [30] Nachum S, Fleck NA (2011) The microstructure and mechanical properties of ball-milled stainless steel powder: the effect of hot-pressing vs. laser sintering. *Acta Mater* 59:7300–7310. <https://doi.org/10.1016/j.actamat.2011.08.004>
- [31] 35 MS (2016) Materials standards for PM structural parts. 32–35
- [32] Krakhmalev P, Yadroitsava I, Fredriksson G, Yadroitsev I (2015) In situ heat treatment in selective laser melted martensitic AISI 420 stainless steels. *Mater Des* 87:380–385. <https://doi.org/10.1016/j.matdes.2015.08.045>
- [33] Yadroitsev I, Krakhmalev P, Yadroitsava I (2015) Hierarchical design principles of selective laser melting for high quality metallic objects. *Addit Manuf* 7:45–56. <https://doi.org/10.1016/j.addma.2014.12.007>
- [34] Yu J, Wang G, Rong Y (2015) Experimental study on the surface integrity and chip formation in the micro cutting process. *Procedia Manuf* 1:655–662. <https://doi.org/10.1016/j.promfg.2015.09.063>
- [35] Al-Jamal OM, Hinduja S, Li L (2008) Characteristics of the bond in Cu-H13 tool steel parts fabricated using SLM. *CIRP Ann Manuf Technol* 57:239–242. <https://doi.org/10.1016/j.cirp.2008.03.010>
- [36] Vikas KSR, Raghu Ram N, Sai Charan B, Indrakanti SS (2019) Hot pressing of copper and copper-based composites: microstructure and suitability as electrodes for electric discharge machining. *Mater Today Proc* 41:1001–1007. <https://doi.org/10.1016/j.matpr.2020.06.069>
- [37] Milman YV, Golubenko AA, Dub SN (2011) Indentation size effect in nanohardness. *Acta Mater* 59:7480–7487. <https://doi.org/10.1016/j.actamat.2011.08.027>
- [38] Jaoui A, Fauqué B, Rischau CW et al (2018) Departure from the Wiedemann-Franz law in WP2 driven by mismatch in

- T-square resistivity prefactors. *npj Quantum Mater* 3:1–7. <https://doi.org/10.1038/s41535-018-0136-x>
- [39] Oxley P, Goodell J, Molt R (2009) Magnetic properties of stainless steels at room and cryogenic temperatures. *J Magn Magn Mater* 321:2107–2114. <https://doi.org/10.1016/j.jmmm.2009.01.002>
- [40] Harvey PD (1982) Engineering properties of steel. ASM International, pp 245–430
- [41] Cho HJ, Kim YJ, Erb U (2018) Thermal conductivity of copper-diamond composite materials produced by electrodeposition and the effect of TiC coatings on diamond particles. *Compos Part B Eng* 155:197–203. <https://doi.org/10.1016/j.compositesb.2018.08.014>
- [42] Barbero EJ (2017) Introduction to composite materials design, 3rd edn. CRC Press
- [43] Chen X, Sun C, Liu C, Fu L (2019) A four-probe method using different probe spacings for measurement and exact reconstruction of parallel profiles. *Appl Sci* 9(23):5216. <https://doi.org/10.3390/app9235216>
- [44] Harter JR, Palmer TS, Greaney PA (2020) Predicting mesoscale spectral thermal conductivity using advanced deterministic phonon transport techniques. *Advances in heat transfer*. Elsevier, pp 335–488
- [45] Giri A, Hopkins PE (2020) A review of experimental and computational advances in thermal boundary conductance and nanoscale thermal transport across solid interfaces. *Adv Funct Mater*. <https://doi.org/10.1002/adfm.201903857>
- [46] Zhao Y, Zeng X, Ren L et al (2021) Heat conduction of electrons and phonons in thermal interface materials. *Mater Chem Front* 5:5617–5638. <https://doi.org/10.1039/d0qm01136c>
- [47] Vincent C, Silvain JF, Heintz JM, Chandra N (2012) Effect of porosity on the thermal conductivity of copper processed by powder metallurgy. *J Phys Chem Solids* 73:499–504. <https://doi.org/10.1016/j.jpcs.2011.11.033>
- [48] Hasselman DPH, Johnson LF (1987) Effective thermal conductivity of composites with interfacial thermal barrier resistance. *J Compos Mater* 21:508–515. <https://doi.org/10.1177/002199838702100602>
- [49] Nan CW, Birringer R, Clarke DR, Gleiter H (1997) Effective thermal conductivity of particulate composites with interfacial thermal resistance. *J Appl Phys* 81:6692–6699. <https://doi.org/10.1063/1.365209>

Publisher's Note Springer Nature remains neutral with regard to jurisdictional claims in published maps and institutional affiliations.